

Spin orbit torques in Pt-based heterostructures with van der Waals interface

Qian Chen(陈倩), Weiming Lv(吕伟明), Shangkun Li(李尚坤), Wenxing Lv(吕文星), Jialin Cai(蔡佳林), Yonghui Zhu(朱永慧), Jiachen Wang(王佳晨), Rongxin Li(李荣鑫), Baoshun Zhang(张宝顺), and Zhongming Zeng(曾中明)
Citation: Chin. Phys. B, 2021, 30 (**9**): 097506. DOI: 10.1088/1674-1056/ac0908
Journal homepage: http://cpb.iphy.ac.cn; http://iopscience.iop.org/cpb

What follows is a list of articles you may be interested in

Effect of hydrogen plasma implantation on the micro-structure and magnetic properties of hcp-$Co_{80}{}^{57}Fe_4Ir_{16}$ thin films

Hui Wang(王辉), Meng Wu(吴猛), Haiping Zhou(周海平), Bo Zhang(张博), Shixin Hu(胡世欣), Tianyong Ma(马天勇), Zhiwei Li(李志伟), Liang Qiao(乔亮), Tao Wang(王涛), and Fashen Li(李发伸)
Chin. Phys. B, 2021, 30 (**5**): 057505. DOI: 10.1088/1674-1056/abe0c3

Experiments and SPICE simulations of double MgO-based perpendicular magnetic tunnel junction

Qiuyang Li(李求洋), Penghe Zhang(张蓬鹤), Haotian Li(李浩天), Lina Chen(陈丽娜), Kaiyuan Zhou(周恺元), Chunjie Yan(晏春杰), Liyuan Li(李丽媛), Yongbing Xu(徐永兵), Weixin Zhang(张卫欣), Bo Liu(刘波), Hao Meng(孟浩), Ronghua Liu(刘荣华), and Youwei Du(都有为)
Chin. Phys. B, 2021, 30 (**4**): 047504. DOI: 10.1088/1674-1056/abdea2

Electrical transport and optical properties of Cd_3As_2 thin films

Yun-Kun Yang(杨运坤), Fa-Xian Xiu(修发贤), Feng-Qiu Wang(王枫秋), Jun Wang(王军), Yi Shi(施毅)
Chin. Phys. B, 2019, 28 (**10**): 107502. DOI: 10.1088/1674-1056/ab3a91

Two-dimensional transport and strong spin-orbit interaction in $SrMnSb_2$

Jiwei Ling(凌霁玮), Yanwen Liu(刘彦闻), Zhao Jin(金昭), Sha Huang(黄沙), Weiyi Wang(王伟懿), Cheng Zhang(张成), Xiang Yuan(袁翔), Shanshan Liu(刘姗姗), Enze Zhang(张恩泽), Ce Huang(黄策), Raman Sankar, Fang-Cheng Chou, Zhengcai Xia(夏正才), Faxian Xiu(修发贤)
Chin. Phys. B, 2018, 27 (**1**): 017504. DOI: 10.1088/1674-1056/27/1/017504

Interplay of Rashba effect and spin Hall effect in perpendicular Pt/Co/MgO magnetic multilayers

Yun-Chi Zhao(赵云驰), Guang Yang(杨光), Bo-Wen Dong(董博闻), Shou-Guo Wang(王守国), Chao Wang(王超), Young Sun(孙阳), Jing-Yan Zhang(张静言), Guang-Hua Yu(于广华)
Chin. Phys. B, 2016, 25 (**7**): 077501. DOI: 10.1088/1674-1056/25/7/077501

SPECIAL TOPIC — Two-dimensional magnetic materials and devices

Spin orbit torques in Pt-based heterostructures with van der Waals interface*

Qian Chen(陈倩)[1], Weiming Lv(吕伟明)[1,2], Shangkun Li(李尚坤)[1], Wenxing Lv(吕文星)[1,3], Jialin Cai(蔡佳林)[1,2], Yonghui Zhu(朱永慧)[1], Jiachen Wang(王佳晨)[1], Rongxin Li(李荣鑫)[1], Baoshun Zhang(张宝顺)[1], and Zhongming Zeng(曾中明)[1,2,†]

[1] *Key Laboratory of Multifunctional Nanomaterials and Smart Systems, Suzhou Institute of Nano-Tech and Nano-Bionics, Chinese Academy of Sciences, Suzhou* 215123, *China*

[2] *Nanchang Nano-Devices and Technologies Division, Suzhou Institute of Nano-Tech and Nano-Bionics, Chinese Academy of Sciences, Nanchang* 330200, *China*

[3] *Physics Laboratory, Industrial Training Center, Shenzhen Polytechnic, Shenzhen* 518055, *China*

(Received 26 April 2021; revised manuscript received 3 June 2021; accepted manuscript online 8 June 2021)

Spin orbit torques (SOTs) in ferromagnet/heavy-metal heterostructures have provided great opportunities for efficient manipulation of spintronic devices. However, deterministically field-free switching of perpendicular magnetization with SOTs is forbidden because of the global two-fold rotational symmetry in conventional heavy-metal such as Pt. Here, we engineer the interface of Pt/Ni heterostructures by inserting a monolayer $MoTe_2$ with low crystal symmetry. It is demonstrated that the spin orbit efficiency, as well as the out-of-plane magnetic anisotropy and the Gilbert damping of Ni are enhanced, due to the effect of orbital hybridization and the increased spin scatting at the interface induced by $MoTe_2$. Particularly, an out-of-plane damping-like torque is observed when the current is applied perpendicular to the mirror plane of the $MoTe_2$ crystal, which is attributed to the interfacial inversion symmetry breaking of the system. Our work provides an effective route for engineering the SOT in Pt-based heterostructures, and offers potential opportunities for van der Waals interfaces in spintronic devices.

Keywords: spin orbit torque, $MoTe_2$, van der Waals interface, crystal symmetry

PACS: 75.70.Tj, 75.70.−I, 71.70.Ej **DOI:** 10.1088/1674-1056/ac0908

1. Introduction

The current-induced manipulation of magnetization realized by spin–orbit torques (SOTs) in ferromagnet/heavy-metal (FM/HM) heterostructures is one of the most active research areas in spintronics.[1,2] SOT arising from the transfer of orbital angular momentum from the lattice to the spin system, is determined by the spin–orbit coupling (SOC) in the HM and at the interface of FM/HM. Due to the limited SOT efficiency and the two-fold rotational symmetry of traditional HM such as Pt, a deterministic and energy-efficient magnetization switching in a system with perpendicular magnetic anisotropy (PMA) is not allowed without an external magnetic field, which greatly limits the application of SOT in low-energy integrated spintronic devices.[3]

Interface engineering of FM/HM gives new opportunities to modulate the SOT effect, which has been confirmed by lots of pioneering works. Qiu *et al.* reported that the large spin absorption at the Ru interface can be employed to manipulate the SOTs in HM/FM/Ru multilayers.[4] Razavi *et al.* modified the conventional SOT heterostructure by inserting a wedged light-metal layer at the HM/FM interface, and achieved the field-free magnetization switching in a PMA system.[5] Recently, based on the strong interfacial orbital hybridization between Pt and Co, enhanced SOT efficiency and induced out-of-plane torques in Pt/Co/Py were reported by Shu *et al.* by inserting an ultrathin Co layer into Pt/Py.[6] However, all of these works require strict control of film thickness, which puts forward high requirements for the film-deposition techniques. Moreover, it is difficult to control the crystallinity of the metal films especially in the low thickness regime.

Extensive research efforts have been devoted to facilitate the practical use of two-dimensional (2D) van der Waals (vdW) materials in SOT devices.[7] Relying on layered structures, 2D vdW materials are possible to realize smooth surfaces with atomic-scale flatness, which facilitates interface engineering of FM/HM. Moreover, high-quality multilayer structures can be easily achieved by stacking 2D vdW interfaces together with metal films because of the absence of dangling bonds on the surface.[8] Integrating 2D vdW materials in SOT devices has shown many advantages, the most striking of which is the out-of-plane damping-like SOT induced by the low crystal symmetry of 2D vdW materials such as WTe_2[9,10] and $MoTe_2$.[11] This novel observation holds a great promise

*Project supported by the National Natural Science Foundation of China (Grant Nos. 51732010, 51802341, and 12004415), the China Postdoctoral Science Foundation (Grant Nos. 2020M671592, 2019M661965), and the Natural Science Foundation of Jiangsu Province, China (Grant No. BK20200255).

†Corresponding author. E-mail: zmzeng2012@sinano.ac.cn

© 2021 Chinese Physical Society and IOP Publishing Ltd

for field-free switching of the perpendicularly magnetized system. In addition, similar to the effects of spin absorption observed in metal films, Debashis *et al.* reported that the spin Hall efficiency of the ultra-thin Ta can be enhanced by more than 25 times when a monolayer (ML) WSe_2 is inserted as an underlayer of $Ta/Co_{60}Fe_{20}B_{20}$ due to spin absorption effect at the interface.[12] Xie *et al.* demonstrated that the SOT efficiency in $Pt/[Co/Ni]_2$ can be greatly enhanced by introducing a MoS_2 underlayer, which is caused by the orbital hybridization at the interface of Pt/Co due to MoS_2.[13] However, it is still lack of evidence whether the low crystal symmetry of 2D vdW materials can be used in interface engineering of conventional FM/HM heterostructures. Recent studies have shown that the low-symmetry $MoTe_2$ has both a large SOT efficiency and a long spin diffusion length at room temperature, making it an excellent candidate for simultaneous spin generation, transport and detection.[14]

In this paper, the SOT effect based on a multilayer structure consisted of $Pt/MoTe_2/Ni$ is investigated, in which the monolayer 1T′-$MoTe_2$ with low crystal symmetry is used as the insert layer to engineer the interface between Pt and Ni. Although retains bulk inversion symmetry, the 1T′-$MoTe_2$ provides a unique opportunity to study the symmetries and interface relevant spin–orbit torques, because its surface symmetry is limited to just one mirror plane. The SOT efficiency is improved which is rationalized by interfacial engineering effects such as orbital hybridization and the increased interfacial scattering. In addition, an out-of-plane damping-like torque is observed when the current is applied perpendicular to the mirror plane of $MoTe_2$. We attribute this special torque to the symmetry breaking of the system caused by monolayer $MoTe_2$.

2. Materials and methods

To prepare the samples, 2 nm Ti and 4 nm Pt films are deposited onto high resistivity Si/SiO_2wafers by electron beam evaporation (EBE). Pt is employed as a spin source where charge-to-spin conversion is happened due to the spin Hall effect (SHE), and the fresh Pt surface is used to assist the exfoliation of monolayer $MoTe_2$, because the $MoTe_2$/Pt binding is stronger than the corresponding interlayer binding in $MoTe_2$.[15] After the exfoliation, $Si/SiO_2/Ti/Pt/MoTe_2$ is reinstate to the high vacuum chamber in rapid sequence to avoid excessive interface degradation or oxidation, and provide a relatively clean interface for the subsequent Ni (6 nm) deposition by EBE. During the deposition, the base pressure is maintained at about 5×10^{-6} torr. The deposition rate of Ni is well controlled as low as 0.1 Å/s, and the whole process is carried out with a room-temperature water-cooled system. Therefore, the energy of Ni atoms acting on $MoTe_2$ is low enough to avoid damaging the vdW monolayer. Figure 1(a) displays an optical image of the $Pt/MoTe_2/Ni$ heterostructure. Monolayer $MoTe_2$ can be resolved by the optical contrast, which is corroborated by direct topography measurements with an atomic force microscope (AFM), and the 0.8 nm step in the height profile shown in the inset of Fig. 1(a) exactly matches the $MoTe_2$ monolayer thickness. We perform cross-sectional transmission electron microscopy (TEM) imaging on a $Pt/MoTe_2/Ni$ device (Fig. 1(b)) as initially identified by AFM.

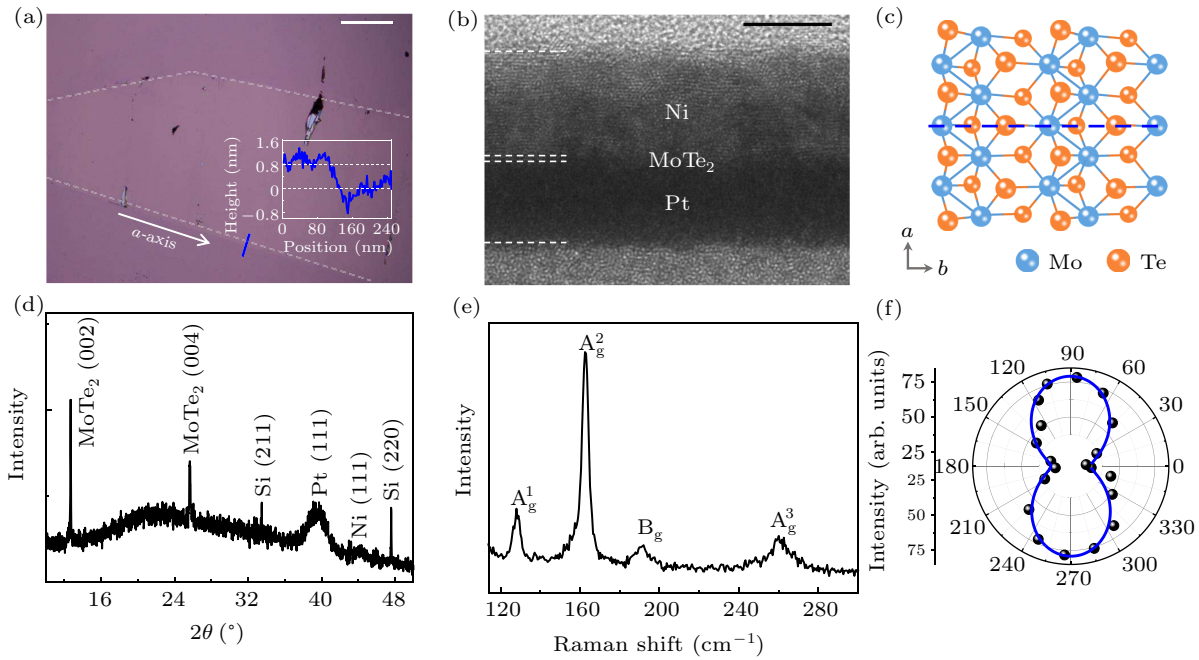


Fig. 1. (a) Optical microscopy image of a $Pt/MoTe_2/Ni$ sample. The scale bar is 20 μm. The line profile drawn across the terrace indicates a step height of ∼ 8 Å. (b) Cross-sectional TEM images of $Pt/MoTe_2/Ni$ multilayer structure. The scale bar is 5 nm. (c) Structure of the 1T′-$MoTe_2$ crystal depicted in the *ab* plane, where the mirror plane is depicted by the dashed blue line. (d) XRD patterns of $Pt/MoTe_2/Ni$. (e) Raman spectra of the exfoliated $MoTe_2$. (f) The polar plots of the angle dependent intensities of A_g mode with the frequency ∼ 265 cm^{-1}. The angle is zero when the excitation laser polarization is parallel to the longitudinal axis of the exfoliated $MoTe_2$.

The delamination of Ni and Pt films is clearly seen, however, monolayer $MoTe_2$ is hardly to be observed because of the limited resolution. Crystal structure of the films is elucidated using x-ray diffraction (XRD). The corresponding XRD patterns of the films are displayed in Fig. 1(d), where crystalline peaks of $MoTe_2$ (002) and (004), Pt (111) and Ni (111) are detected, indicating that the crystal surface of $MoTe_2$ is normal to the *c*-axis with the plate-shaped surface parallel to the *ab* plane. To investigate the crystal quality of the exfoliated $MoTe_2$, Raman spectroscopy with a 532 nm excitation laser is utilized. Characteristic Raman peaks are observed: A_g modes at about 128 cm^{-1}, 163 cm^{-1} and 265 cm^{-1}, B_g mode at about 189 cm^{-1} (Fig. 1(e)), which are in accordance with the Raman shifts predicted from theoretical calculations.[16] Polarized Raman spectroscopy is carried out to confirm the orientation of the crystal axes of $MoTe_2$. The polar plot of the angle dependent intensities of the A_g mode with the frequency ~ 265 cm^{-1} is shown in Fig. 1(f), which is in good agreement with previous studies[17] and proves that the longitudinal axis of the exfoliated $MoTe_2$ is along its *a*-axis (typically perpendicular to the mirror plane of $MoTe_2$, as marked in Fig. 1(c)).

3. Results and discussion

To fabricate Pt/$MoTe_2$/Ni devices for the SOT study, the samples are patterned into micro-strips by electron-beam lithography and Ar ion etching, and electrical connections are made by Ti/Au contact pads. The long axis of the micro-strip is along the *a*-axis of $MoTe_2$, so that the current is applied along the low-symmetry crystal axis of $MoTe_2$, leading to the breaking of inversion symmetry at the interface. Pt/Ni device is also fabricated for comparison. Using the circuit shown in Fig. 2(a), we measure the spin orbit torques by the technique of spin-torque ferromagnetic resonance (ST-FMR).[18] During the measurement, an alternating current I with a fixed frequency f is applied through the device, and a sweeping magnetic field H is applied in the film plane, with the angle ϕ between H and the long axis of the micro-strip kept at 45° unless otherwise indicating. The output power of the microwave signal generator is 18 dBm. All the measurements are performed at room temperature. In ST-FMR, the torques generated by the current excite the magnetic moment away from equilibrium and cause it to precess, creating a time-dependent change in the resistance of the device due to the anisotropic magnetoresistance (AMR) in Ni. The mixing between the applied alternating current and the oscillating resistance further generates a mixing voltage V_{mix} due to the spin torque diode effect as given by[18,19]

$$V_{mix} = -\frac{1}{4}\frac{dR}{d\phi}\frac{\gamma I_{rf}\cos\phi}{\Delta H 2\pi\,(df/dH)|_{H=H_{res}}}\left[SF_S(H)+AF_A(H)\right], \tag{1}$$

where I_{rf} is the microwave current in the device, R and γ are the resistance and the gyromagnetic ratio of Ni, H_{res} is

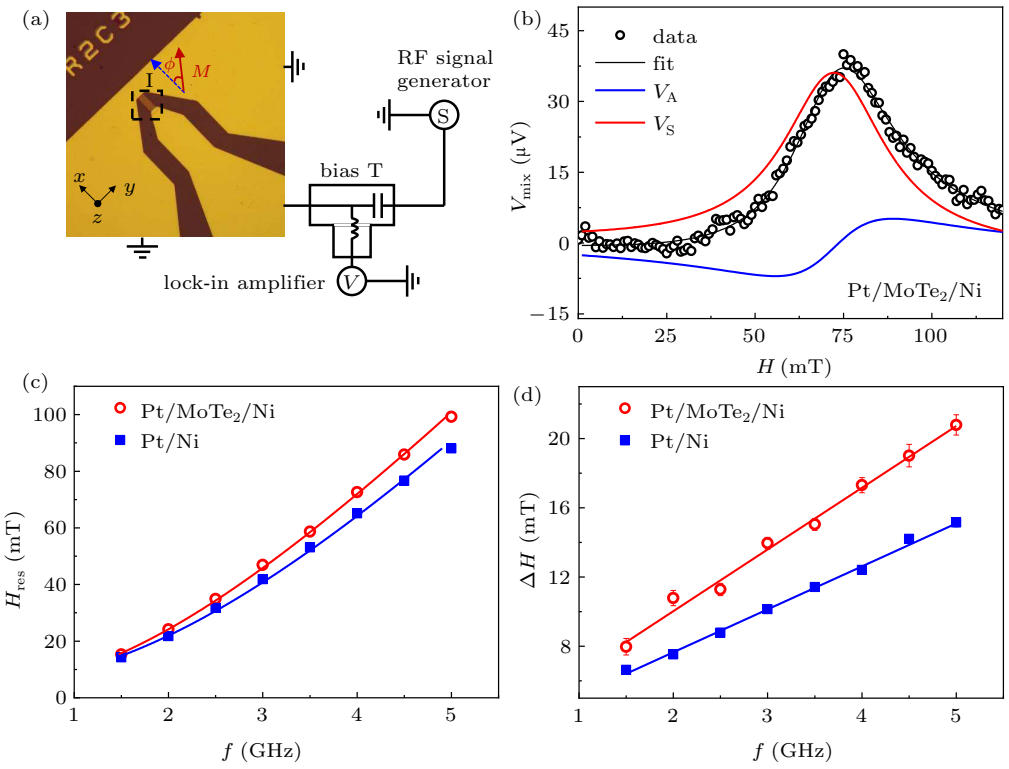


Fig. 2. (a) Optical images of the device including contact pads, with the circuit used for ST-FMR measurement. (b) Measured ST-FMR spectra for Pt/$MoTe_2$/Ni, with the magnetization oriented at 45° relative to the current direction and $f = 4$ GHz. The lines are fits to Eq. (1) showing the symmetric V_S and antisymmetric V_A resonance components. (c) Frequency dependence of the resonance field for Pt/Ni and Pt/$MoTe_2$/Ni devices. The solid lines represent the theoretical fitting using the Kittle equation. (d) The linewidth ΔH extracted from the fitting of the ST-FMR signal as a function of the resonant frequency f. The solid lines are the linear fittings.

the resonant field, ΔH is the half width at half maximum. $F_S(H) = \Delta H^2 / \left[\Delta H^2 + (H - H_{res})^2\right]$ is a symmetric Lorenzian function centered at the resonant field, and $F_A(H) = F_S(H)(H - H_0)/\Delta H$ is an antisymmetric Lorentzian. S and A are the weight factors for the symmetric and antisymmetric FMR, which are proportional to the spin current density J_S and charge current density J_C, respectively. From the line-shape parameters, the SOT efficiency ξ_{SOT} can be evaluated using the standard line-shape analysis method, as given by[18,19]

$$\xi_{SOT} = td\frac{S}{A}\frac{e\mu_0 M_s}{\hbar}\sqrt{1 + (4\pi M_{eff}/H_{res})}, \quad (2)$$

where μ, e, t, d, M_s, and M_{eff} are the magnetic permeability in free space, electronic charge, thickness of ferromagnetic layer, thickness of nonmagnetic layer, saturation magnetization and effective magnetization of Ni, respectively.

Frequency dependences of H_{res} and ΔH are illustrated in Figs. 2(c) and 2(d), respectively, where we find that both the resonance field and linewidth of Ni are increased after the insertion of monolayer $MoTe_2$ especially at high frequencies, implying the regulation of Ni magnetism by $MoTe_2$. The effective magnetization M_{eff} is extracted by fitting the f versus H_{res} data to the Kittel equation (as shown in Fig. 2(c)), $f = (\gamma/2\pi)[(H_{res} + H_k)(H_{res} + H_k + 4\pi M_{eff})]^{1/2}$.[20] Here, H_k denotes the in-plane magnetic anisotropy which is close to zero, and M_{eff} incorporates the M_s and the surface anisotropy field H_s, that is $4\pi M_{eff} = 4\pi M_s - H_s$.[21] $H_s > 0$ is defined as surface anisotropy in the film normal and $H_s < 0$ stands for the surface anisotropy in the film plane. The extracted $4\pi M_{eff}$ of Pt/$MoTe_2$/Ni is 232.43 ± 4.40 mT, smaller than the value extracted from Pt/Ni (286.39 ± 7.94 mT). The reduction of M_{eff} in Pt/$MoTe_2$/Ni indicates either a decrease of M_s or an increased PMA in Ni induced by $MoTe_2$. Previous work has shown that 2D transition-metal dichalcogenides should not result in a change in M_s,[11,22] but are likely to enhance the PMA of the magnetic layer due to the modification of the orbital hybridization.[13] Accordingly, compared with Pt/Ni bilayers, the increased PMA field in Pt/$MoTe_2$/Ni is about 53.96 mT, which may arise from the interfacial d–d orbital hybridization of Pt, Mo and Ni.[6,13] Using the fitted values of M_{eff}, the SOT efficiency of Pt/Ni is calculated as 0.125 ± 0.011, close to the value reported by Bose *et al.*[23] but slightly higher compared to other reports[24] which can be attributed to the impurity present in Pt for different lab conditions. Comparatively, the SOT efficiency of Pt/$MoTe_2$/Ni is extracted as 0.197 ± 0.016, much larger than the value extracted from Pt/Ni. Such an enhancement of ξ_{SOT} may be related to the increased spin–orbital coupling (SOC) caused by interfacial d–d orbital hybridization.[6,13] On the other hand, recently, Novakov *et al.* demonstrated that insertion of up to two monolayers of WSe_2 is able to enhance the spin transfer torques in a Rashba system by up to 3 times,[25] indicating that low layer count 2D vdW materials can be used as an interfacial scattering promoter in heterostructure interfaces without quenching the original polarization. Although there is absent of direct evidences whether $MoTe_2$ fits the Rashba system or not,[26] the increased scattering will enhance the spin fluctuation at the interface as well, which amplifies the spin current transmission between Pt and Ni and then improve the SOT efficiency in Pt/$MoTe_2$/Ni device.[27,28]

Figure 2(d) shows the linear relationships between ΔH and f, which are well fitted with the equation $\Delta H = \Delta H_0 + 2\pi f\alpha/\gamma$,[29] where α is the Gilbert damping of Ni. The linewidth contribution from inhomogeneity can be estimated from the value of ΔH_0. Here, similar values of ΔH_0 (~ 25 Oe) for Pt/Ni and Pt/$MoTe_2$/Ni are extracted, suggesting that the insert of $MoTe_2$ does not cause significant inhomogeneity in Ni. Fitting results are listed in Table 1. Gilbert damping of Pt/Ni device is 0.0695 ± 0.0018, and increases to 0.0999 ± 0.0050 after inserting monolayer $MoTe_2$. The increased damping indicates the additional loss of the spin angular momentum dissipated in Ni. According to the spin pumping theory raised by Tserkovnyak *et al.*,[30,31] a moving magnetization vector causes pumping of spins into adjacent nonmagnetic layers. This spin transfer affects the magnetization dynamics similar to the Landau–Lifshitz–Gilbert phenomenology, and an additional Gilbert damping is induced when the nonmagnetic layers efficiently relax the injected spins. Here, in Pt/$MoTe_2$/Ni, spin currents generated from Ni are relaxed in Pt, and the $MoTe_2$ may act as a scattering promoter, increasing the spin transport efficiency at the interface which is similar to the model provided by Novakov *et al.*[25] and Lee *et al.*[27,28] However, further studies regarding to the spin pumping effect in systems with 2D vdW interfaces are still needed.

Table 1. The $4\pi M_{eff}$, α and ξ_{SOT} extracted from ST-FMR measurements.

Device	$4\pi M_{eff}$ (mT)	α	ξ_{SOT}
Pt/Ni	286.39 ± 7.94	0.0695 ± 0.0018	0.125 ± 0.011
Pt/$MoTe_2$/Ni	232.43 ± 4.40	0.0999 ± 0.0050	0.197 ± 0.016

To determine the effect of interfacial symmetry breaking induced by $MoTe_2$, we analyze the extracted fit parameters V_S and V_A as functions of the applied field angle. Representative data for Pt/$MoTe_2$/Ni and Pt/Ni are shown in Figs. 3(a)–3(d). Because of the high-symmetry of Pt, the generated spin orbit torques by Pt are consist of an out-of-plane field-like torque, $\tau_A \propto \hat{m} \times \hat{y}$, and an in-plane damping-like torque, $\tau_S \propto \hat{m} \times (\hat{m} \times \hat{y})$, so that V_A and V_S conform to the angle dependency of $\sin(2\phi)\cos(\phi)$.[32] Note that we define the applied current as always being in the $\hat{x}$ direction (Fig. 2(a)). Recent studies have demonstrated that, apart from τ_A and τ_S, an out-of-plane damping-like torque τ_B is also allowed when the

system has a single mirror symmetry and the current is applied perpendicular to this mirror plane,[9–11] as is the case for our Pt/$MoTe_2$/Ni device. To extract τ_B, we fit the angular dependence of V_A by the simple addition of a term ΔV_A (Fig. 3(b)) proportional to $\sin(2\phi)$,[9]

$$V_A(\phi) = A\cos(\phi)\sin(2\phi) + B\sin(2\phi), \tag{3}$$

where the fit parameter B represents $\tau_B \propto \hat{m} \times (\hat{m} \times \hat{z})$. The ratio $B/A = 0.104 \pm 0.037$, which is about three-times smaller than the value obtained in the monolayer $MoTe_2$/Py structure reported by Stiehl *et al.*[11] This is reasonable since both Pt and $MoTe_2$ contribute to τ_A and τ_S in Pt/$MoTe_2$/Ni device.

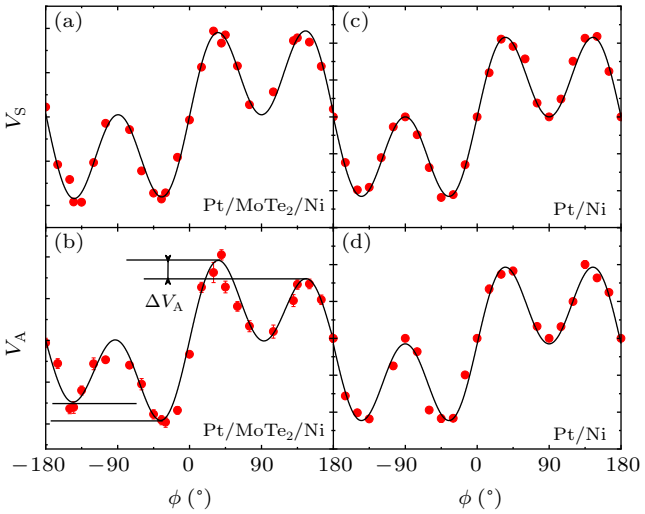


Fig. 3. Dependence on the applied field angle for the (a) symmetric, V_S, and (b) antisymmetric, V_A, components of mixing voltage for Pt/$MoTe_2$/Ni, with current applied parallel to the *a*-axis of $MoTe_2$. (c) V_S and (d) V_A of mixing voltage for Pt/ Ni. The frequency of the microwave during measurement is 4 GHz.

To further demonstrate the symmetry dependence of τ_B, Pt/$MoTe_2$/Ni device with current applied parallel to the *b*-axis of $MoTe_2$ is studied. Figure 4 shows the antisymmetric ST-FMR component V_A as a function of ϕ, where we find no evidence of ΔV_A since τ_B is forbidden by symmetry in this case.[11]

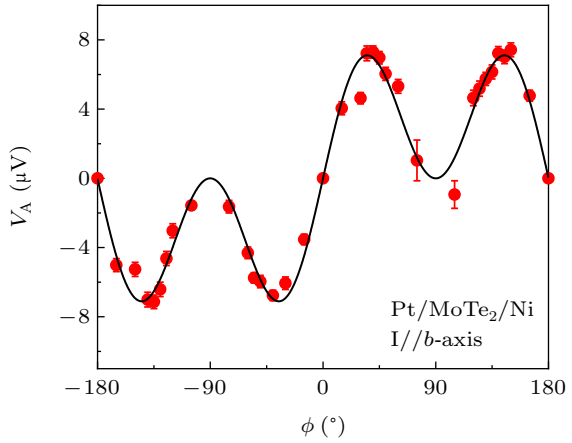


Fig. 4. Antisymmetric ST-FMR component V_A for Pt/$MoTe_2$/Ni as a function of in-plane magnetic-field angle, with current applied parallel to the *b*-axis of $MoTe_2$. The microwave frequency is 4 GHz.

4. Conclusions

In summary, we have demonstrated that it is feasible to engineer the interface of conventional Pt based FM/HM heterostructures by inserting monolayer 2D $MoTe_2$ with low crystal symmetry. The out-of-plane magnetic anisotropy of Ni is increased due to the interfacial d–d orbital hybridization of Pt, Mo and Ni. The Gilbert damping of Ni is enhanced from 0.0695 in Pt/Ni to 0.0999 in Pt/$MoTe_2$/Ni due to the additional loss of the spin angular momentum caused by $MoTe_2$. The SOT efficiency of Pt/$MoTe_2$/Ni is up to 0.197, much larger than that of Pt/Ni. We suspect that the improved SOT efficiency is related to the interfacial orbital hybridization and the enhanced interfacial scattering of spin current induced by monolayer $MoTe_2$. Particularly, an out-of-plane damping-like torque is induced and shows dependence on the interfacial inversion symmetry of the system. When the current is applied along the low-symmetry crystal axis of $MoTe_2$, the out-of-plane damping-like torque is observed, and when the current is applied parallel to the mirror plane, it is invisible. Our results suggest a strategy for achieving efficient manipulation of magnetic devices with PMA. To date, various approaches for field-free SOT-induced magnetization switching of PMA structures have been proposed and demonstrated, for example, switching using a wadge oxide capping layer,[33] a polarized ferroelectric substrate,[34] lateral SOT,[35] introducing an interlayer coupling or an exchange bias field.[36,37] Compared with these previous methods, 2D vdW interface induced out-of-plane SOT broadens the scope of material engineering for conventional Pt-based SOT devices, and the efficiency of SOT is improved coupled with the additional symmetry breaking, making it a promising candidate for magnetic memory and logic devices driven by SOT.

References

[1] Han X, Wang X, Wan C, Yu G and Lv X 2021 *Appl. Phys. Lett.* **118** 120502
[2] Cao Y, Xing G, Lin H, Zhang N, Zheng H and Wang K 2020 *iScience* **23** 101614
[3] Zheng Z, Zhu D, Zhang K, Feng X, He Y, Chen L, Zhang Z, Liu D, Zhang Y, Amiri P and Zhao W 2020 *Chin. Phys. B* **29** 078505
[4] Qiu X, Legrand W, He P, Wu Y, Yu J, Ramaswamy R, Manchon A and Yang H 2016 *Phys. Rev. Lett.* **117** 217206
[5] Razavi A, Wu H, Shao Q, Fang C, Dai B, Wong K, Han X, Yu G and Wang K 2020 *Nano Lett.* **20** 3703
[6] Shu X, Zhou J, Liu L, Lin W, Zhou C, Chen S, Xie Q, Ren L, Yu X, Yang H and Chen J 2020 *Phys. Rev. Appl.* **14** 054056
[7] Liu Y and Shao Q 2020 *ACS Nano* **14** 9389
[8] Kahn E, Liu M, Zhang T, Liu H, Fujisawa K, Bepete G, Ajayan P and Terrones M 2020 *Mater. Today* **37** 74
[9] Macneill D, Stiehl G, Guimaraes M, Buhrman R, Park J and Ralph D 2017 *Nat. Phys.* **13** 300
[10] Macneill D, Stiehl G, Guimaraes M, Reynolds N, Buhrman R and Ralph D 2017 *Phys. Rev. B.* **96** 054450
[11] Stiehl G, Li R, Gupta V, Baggari I, Jiang S, Xie H, Kourkoutis L, Mak K, Shan J, Buhrman R and Ralph D 2019 *Phys. Rev. B* **100** 184402
[12] Debashis P, Hung T and Chen Z 2020 *npj 2D Mater. Appl.* **4** 18

[13] Xie Q, Lin W, Yang B, Shu X, Chen S, Liu L, Yu X, Breese M, Zhou T, Yang M, Zhang Z, Wang S, Yang H, Chai J, Han X and Chen J 2019 *Adv. Mater.* **31** 1900776

[14] Song P, Hsu C, Vignale G, Zhao M, Liu J, Deng Y, Fu W, Liu Y, Zhang Y, Pereira V and Loh K 2020 *Nat. Mater.* **19** 292

[15] Huang Y, Pan Y, Yang R, *et al*. 2020 *Nat. Commun.* **11** 2453

[16] Kan M, Nam H, Lee Y and Sun Q 2015 *Phys. Chem. Chem. Phys.* **17** 14866

[17] Wang J, Luo X, Li S, Verzhbitskiy I, Zhao W, Wang S, Quek S and Eda G 2017 *Adv. Funct. Mater.* **27** 1604799

[18] Liu L, Moriyama T, Ralph D and Buhrman R 2011 *Phys. Rev. Lett.* **106** 036601

[19] Yang W, Wei J, Wan C, Xing Y, Yan Z, Wang X, Fang C, Guo C, Yu G and Han X 2020 *Phys. Rev. B* **101** 064412

[20] Herring C and Kittel C 1951 *Phys. Rev.* **81** 869

[21] Kageyama Y, Tazaki Y, An H, Harumoto T, Gao T, Shi J and Ando K 2019 *Sci Adv.* **5** eaax4278

[22] Husain S, Chen X, Gupta R, Behera N, Kumar P, Edvinsson T, García-Sanchez F, Brucas R, Chaudhary S, Sanyal B, Svedlindh P and Kumar A 2020 *Nano Lett.* **20** 6372

[23] Bose A, Singh H, Kushwaha V, Bhuktare S, Dutta S and Tulapurkar A 2018 *Phys. Rev. Appl.* **9** 014022

[24] Hayashi H, Musha A, Sakimura H and Ando K 2020 *Phys. Rev. Research* **3** 013042

[25] Novakov S, Jariwala B, Vu N, Kozhakhmetov A, Robinson J and Heron J 2021 *ACS Appl. Mater. Interfaces.* **13** 13744

[26] Zhao Y, Yang G, Dong B, Wang S, Wang C, Sun Y, Zhang J and Yu G 2016 *Chin. Phys. B* **25** 077501

[27] Lee W, Park N, Kim G, Kang M, Choi J, Choi K, Jang H, Saitoh E and Lee S 2021 *Nano Lett.* **21** 189

[28] Lee W, Kang M, Kim G, Park N, Choi K, Le C, Rashid M, Saitoh E, Kim Y and Lee S 2021 *ACS Appl. Mater. Interfaces* **13** 15783

[29] Yin Y, Pan F, Ahlberg M, Ranjbar M, Durrenfeld P, Houshang A, Haidar M, Bergqvist M, Zhai Y, Dumas R, Delin A and Akerman J 2015 *Phys. Rev. B* **92** 024427

[30] Tserkovnyak Y, Brataas A and Bauer G 2002 *Phys. Rev. Lett.* **88** 117601

[31] Tserkovnyak Y, Brataas A and Bauer G 2002 *Phys. Rev. B* **66** 224403

[32] Garello K, Miron I, Avci C, Freimuth F, Mokrousov Y, Blugel S, Auffret S, Boulle O, Gaudin G and Gambardella P 2013 *Nat. Nanotechnol.* **8** 587

[33] Yu G, Upadhyaya P, Fan Y, Alzate J, Jiang W, Wong K, Takei S, Bender S, Chang L, Jiang Y, Lang M, Tang J, Wang Y, Tserkovnyak Y, Amiri P and Wang K 2014 *Nat. Nanotechnol.* **9** 548

[34] Cai K, Yang M, Ju H, Wang S, Ji Y, Li B, Edmonds K, Sheng Y, Zhang B, Zhang N, Liu S, Zheng H and Wang K 2017 *Nat. Mater.* **16** 712

[35] Cao Y, Sheng Y, Edmonds K, Ji Y, Zheng H and Wang K 2020 *Adv. Mater.* **32** 1907929

[36] Lau Y, Betto D, Rode K, Coey J and Stamenov P 2016 *Nat. Nanotechnol.* **11** 758

[37] Fukami S, Zhang C, Gupta S, Kurenkov A and Ohno H 2016 *Nat. Mater.* **15** 535